Generation of excited K bands in heavy nuclei

B. Buck,[1] A. C. Merchant,[1] and S. M. Perez[2,3]
[1]*Department of Physics, University of Oxford, Theoretical Physics, 1 Keble Road, Oxford OX1 3NP, UK*
[2]*Department of Physics, University of Cape Town, Private Bag, Rondebosch 7700, South Africa*
[3]*iThemba LABS, P.O. Box 722, Somerset West 7129, South Africa*
(Received 16 April 2011; revised manuscript received 6 August 2011; published 8 September 2011)

It is known that coupling an intrinsic excitation of integer spin and positive parity I^+ to a rotor having a degenerate set of states $L^\pi = 0^+, 2^+, 4^+, \ldots$, generates a series of K bands. A given value of I^+ gives rise to several bands labeled by $K^+ = 0^+, 1^+, 2^+, \ldots, I^+$, that is, a total of $(I + 1)$ such bands, in the spectrum of the combined system. We discuss how a binary cluster model of an excited core orbited by a spinless cluster can approximate these conditions. A crucial point is that the radial wave functions of relative motion are very similar for low L, and their radial coupling integrals even more so, such that the wave functions play the model role of a common intrinsic state for the lowest excited states of the system. If the core has a 0^+ ground state and a low-lying 2^+ excited state, then lifting the degeneracy leads to a ground state $K^+ = 0^+$ band and low-lying excited $K^+ = 0^+, 1^+$, and 2^+ bands. Although these are all seen in light nuclei, the $K^+ = 1^+$ band is conspicuous by its apparent absence in heavy nuclei, and we urge experimental groups to reexamine their data for signs of it.

DOI: 10.1103/PhysRevC.84.034310 PACS number(s): 21.10.Re, 21.60.Ev, 21.60.Gx, 27.90.+b

I. INTRODUCTION

Quasirotational ground-state bands of states with angular momentum sequences $J^+ = 0^+, 2^+, 4^+, \ldots$, are observed in even-even nuclei across the Periodic Table. They are present in light nuclei, such as ^{8}Be [1,2], ^{16}O [1,3], and ^{24}Mg [1,4] through regions of strong deformation in the rare-earth region and beyond into the trans-Pb and Actinide nuclei [1]. Excited sequences of states having angular momenta $J = K, (K + 1), (K + 2), \ldots$, where K is an integer (and the parity may be positive or negative) are also commonly observed.

There are complementary geometric and algebraic descriptions of these phenomena. The basis for the traditional geometric explanation has been provided by the collective-rotational model of Bohr and Mottelson [5]. In this model K bands arise when the Hamiltonian is split into intrinsic and rotational parts and the adiabatic approximation is made for the rotational part. Then an appropriately chosen intrinsic state of the even-even core $\Phi_K(q)$ and its time-reversed partner $\Phi_{\bar{K}}(q)$ couple with axially symmetric rotor functions having rotational and reflectional symmetries with respect to a body-fixed OZ' axis and $OX'Y'$ plane to produce wave functions of the form

$$\Psi_{KJM} = \sqrt{\frac{2J+1}{16\pi^2}}\big[\Phi_K(q)D^J_{MK}(\omega) + (-1)^{J+K}\Phi_{\bar{K}}(q)D^J_{M-K}(\omega)\big]. \quad (1)$$

In an alternative algebraic approach, independent of any symmetry assumptions, Brink *et al.* [6] showed that K bands also emerge when a particle of spin j is coupled to a degenerate set of $L^\pi = 0^+, 2^+, 4^+, \ldots$, states having a common intrinsic component. This approach is particularly suited to a discussion of rotational motion within a binary cluster model and we show below that the coupling of a 2^+ state to a rotor produces a triplet of bands having $K^\pi = 0^+, 1^+$, and 2^+ at rather similar excitation energies. It is tempting to identify the predicted 0^+ and 2^+ bands with the beta and gamma bands seen at about 1 MeV in many actinide nuclei. If this is correct we expect an accompanying 1^+ band as a generic feature of the spectrum. This structure can be visible through the explicit observation of a 1^+ state or through seeing pairs of states of given odd J^+ close to each other in energy. This is in marked contrast to the traditional Bohr-Mottelson picture where, although one can get a 1^+ band as a two quasi-particle state, that would not be a generic feature of the spectrum. In particular, one never gets 1^+ bands in the Bohr-Mottelson picture by coupling two 2^+ phonons [7]. Failure to observe a 1^+ band accompanying 0^+ and 2^+ bands at similar excitation energies, as a common feature, will indicate that our model fails to describe an important characteristic of heavy deformed nuclei.

Theoretical studies of positive parity bands in the actinide nuclei were also presented within the cranked random phase approximation (RPA) [8–11], the collective model [12–14], the interacting boson approximation [15,16], the variable moment of inertia model [17], and the alpha particle cluster model [18].

In this article we shall examine the conditions under which K bands are produced in a binary cluster model and indicate that a deep potential in which low-L wave functions undergo many oscillations is particularly propitious for their generation. In the next section we outline a suitable form of the cluster-core potential and observe that its radial wave functions have very little dependence on L, particularly in the region of the nuclear surface. We go on to calculate overlap and radial coupling integrals and compare these with equivalent expressions for wave functions generated by a three-dimensional harmonic oscillator potential. This leads on to a discussion of the generation of K bands, the lifting of degeneracy in the weak and strong coupling limits, and a strong suggestion that $K^+ = 1^+$ bands ought to be widespread in heavier nuclei. Finally, after a brief discussion of the electromagnetic properties of these bands, we summarize our conclusions.

II. CLUSTER MODEL

The system under study is an actinide nucleus, modeled as two even-even subnuclei, a core A_1 and a cluster A_2 separated by a distance $\mathbf{R}$, interacting with each other through a deep, local potential $V(R)$ composed of a nuclear part $V_N(R)$ and a Coulomb part $V_C(R)$. The nuclear component may be conveniently parametrized in the form [19]

$$V_N(R) = -V_0\left\{\frac{x}{\{1+\exp[(R-R_0)/a)]\}} + \frac{1-x}{\{1+\exp[(R-R_0)/3a]\}^3}\right\}. \quad (2)$$

In the following we shall use the parameter set $T1$ for this potential employed in a previous systematic study of the actinide region [20], namely

$$V_0 = 56.6A_2 \text{ MeV}, \quad a = 0.75 \text{ fm}, \quad \text{and} \quad x = 0.36. \quad (3)$$

The Coulomb component $V_C(R)$ is taken as that acting between a uniformly charged spherical core of radius R_0 and a point cluster [20].

Writing $H_0(\mathbf{R})$ for the Hamiltonian of the relative motion of core and cluster and $H_1(\boldsymbol{\xi})$ for the internal Hamiltonian of the core, we have

$$H_0(\mathbf{R})\Phi_{GnL}(\mathbf{R}) = E_{GnL}\Phi_{GnL}(\mathbf{R}) = E_{GnL}\frac{u_{GnL}(R)}{R}Y_{LM}(\theta,\phi), \quad (4)$$

and

$$H_1(\boldsymbol{\xi})\chi_I(\boldsymbol{\xi}) = \epsilon_I\chi_I(\boldsymbol{\xi}). \quad (5)$$

In Eq. (4) the wave functions and energies are labeled by the global quantum number $G = 2n + L$, with n the number of internal nodes in the radial wave function and L the orbital angular momentum. The value of G must be chosen large enough to ensure that the major requirements of the Pauli exclusion principle are satisfied by effectively excluding the cluster nucleons from states occupied by the core nucleons. To this end we follow the prescription of $T1$ [20] and take $G = 5A_2$. Thus, we restrict ourselves to the band of states $L^\pi = 0^+, 2^+, 4^+, \ldots, G^+$ generated by a particular, fixed, even value of G, and from now on drop the subscripts G and n accordingly. In Eq. (5) $\boldsymbol{\xi}$ denotes the internal coordinates of the core and I labels the core states, with $I = 0^+$ the ground state and $I = I^\pi$ an excited state.

We have previously found [21,22] that the multinodal radial wave functions $u_L(R)$ of high n and low L are all very similar in the surface region. This is shown in Fig. 1 for the four actinide nuclei ^{222}Ra [1,23], ^{228}Th [1,24], ^{232}U [1,25], and ^{236}Pu [1,26] modeled as ^{208}Pb + ^{14}C, ^{20}O, ^{24}Ne, and ^{28}Mg, respectively, where we plot the radial wave functions $u_L(R)$ obtained from a numerical solution of the Schrödinger equation for the potential $V(R)$ described above and the L values of 0, 4, 8, 12, 16, and 20. The main differences between the radial wave functions for a given nucleus occur close to the origin and are due to the node number differences. For example, the $L = 0$ wave functions contain $G/2$ nodes while the $L = 20$ wave functions contain ten fewer nodes. This node number mismatch is most clearly visible for the lighter nuclei since they have smaller cluster masses A_2 and correspondingly smaller values of $G/2 = 2.5A_2$ such that a difference of ten nodes represents a larger fractional change. In all cases the node number difference is almost entirely accommodated within a narrow region restricted to the vicinity of the origin. Beyond $R \sim 2.0$ fm the wave functions oscillate in phase with one another, having closely similar amplitudes, so that they are scarcely distinguishable from one another at all.

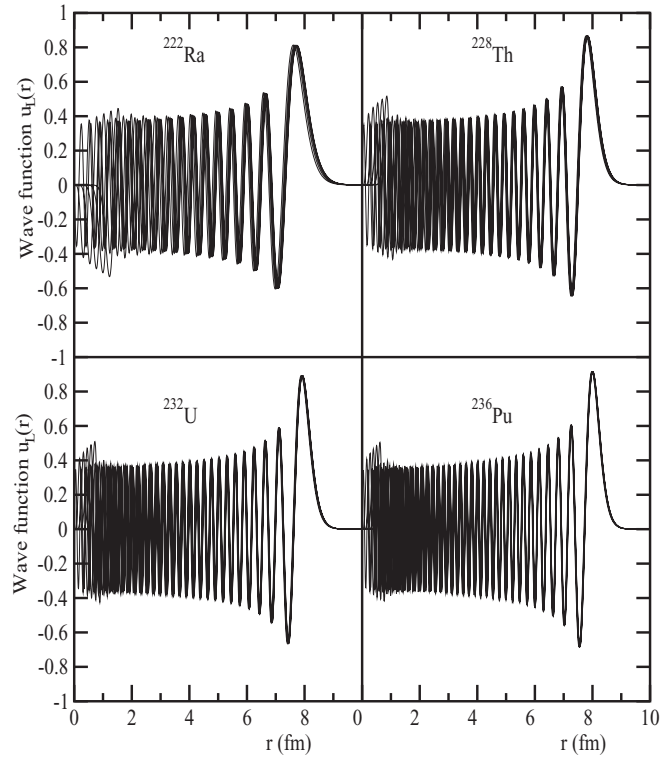

FIG. 1. Radial wave functions for L values of 0, 4, 8, 12, 16, and 20 for the actinide nuclei ^{222}Ra, ^{228}Th, ^{232}U, and ^{236}Pu modeled as ^{208}Pb + ^{14}C, ^{20}O, ^{24}Ne, and ^{28}Mg, respectively, obtained from a numerical solution of the Schrödinger equation. (See text for details of the potential.)

A. Wave-function overlaps

To emphasize the similarity of the radial wave functions we next consider their overlap integrals $I_{nL}^{(m)} = \langle n, L|n', L'\rangle$ for states in the same band (i.e., with a common value of $G = 2n + L$), but node numbers n and $n' = (n - m)$ corresponding to angular momenta L and $L' = L + 2m$, respectively. These are given by

$$I_{nL}^{(m)} = \langle n, L|(n-m), (L+2m)\rangle = \int_0^\infty u_{n,L}(R)u_{(n-m),(L+2m)}(R)\,dR. \quad (6)$$

We find that the similarity of the $I_{nL}^{(m)}$ is a general feature of deep potentials and large values of G. This can be conveniently demonstrated by comparing the numerical results from the potential $V(R)$ described above with equivalent analytic

results for a three-dimensional harmonic oscillator potential for which (see the Appendix for more details)

$$I_{nL}^{(m)} = \langle n, L|(n-m),(L+2m)\rangle = (-1)^m \sqrt{\frac{(n)!}{(n-m)!} \times \frac{\Gamma(n+L+3/2)}{\Gamma(n+L+m+3/2)}}. \quad (7)$$

Tables I and II show a numerical comparison of the overlap integrals for the lightest (^{222}Ra) and heaviest (^{236}Pu) nuclei under consideration, with L and L' ranging between 0 and 20 in steps of two. Similar integrals for ^{228}Th and ^{232}U lie in between the values for the two tabulated nuclei. The numerically calculated overlaps are systematically larger than the oscillator equivalents, and the values of the heavier nucleus are larger than those for the lighter nucleus at the same L and L'. The extreme cases of $L = 0$ overlapped with $L' = 20$ still yield 0.6180 for ^{236} Pu and 0.3419 for ^{222}Ra. Furthermore, these overlap values understate the degree of similarity of the wave functions in the region of the nuclear surface, to which many observable quantities are most sensitive.

B. Radial coupling integrals

Although overlap integrals provide a convenient measure of the similarity of two wave functions they cover a wider range of R, L, and L' than we really require. Our principal concern is with the comparability of radial integrals involving the overlap of a pair of radial wave functions and the radial part of a coupling potential, which is traditionally related to the central nuclear potential of Eqs. (2) and (3) through the relation

$$V_{\text{couple}}(R) = R \times \frac{dV_N}{dR}. \quad (8)$$

Such a coupling potential generally peaks in the nuclear surface, and so the more interesting question concerns how similar are the different wave functions in this region. Also, if attention is restricted to a quadrupole-quadrupole interaction between cluster and core, the wave functions involved in these radial integrals will only differ in their L values by two units, with modified but similar restrictions holding for higher multipoles. Figure 2 illustrates the near constancy of quadrupole-quadrupole radial coupling integrals for the actinide nuclei ^{222}Ra, ^{228}Th, ^{232}U, and ^{236}Pu. Again, equivalent results for three-dimensional harmonic oscillator wave functions and the corresponding coupling potential can be evaluated analytically such that (see the Appendix for more details)

$$\langle n, L|R\frac{dV}{dR}|n-m, L+2m\rangle = I_{nL}^{(m)}[(m+1)(n+L+3/2) - (m-1)(n-m)]\mu\omega^2 b^2, \quad (9)$$

and are represented by the broken line in Fig. 2 for comparison, to emphasize that we are not dealing with a special property of our chosen parametrization of the nuclear potential.

C. Similarities in local wave numbers

Figure 1 shows that the low-L members of a large-G band have similar radial wave functions, particularly in the important surface region, with the similarity increasing with increasing cluster mass A_2. We next show more directly how these characteristics arise by comparing the local wave numbers generated by the cluster model. This is most easily achieved using a harmonic oscillator cluster-core potential for which the local wave number of the L and 0 angular momentum members of a G band are given by

$$k_L(R) = \sqrt{\frac{2\mu}{\hbar^2}\left\{E - V(R) - \frac{\hbar^2 L(L+1)}{2\mu R^2}\right\}} \quad (10)$$

$$= \sqrt{\frac{2\mu}{\hbar^2}\left\{\left(G+\frac{3}{2}\right)\hbar\omega - \frac{1}{2}\mu\omega^2 R^2 - \frac{\hbar^2 L(L+1)}{2\mu R^2}\right\}}, \quad (11)$$

and

$$k_0(R) = \sqrt{\frac{2\mu}{\hbar^2}\left\{\left(G+\frac{3}{2}\right)\hbar\omega - \frac{1}{2}\mu\omega^2 R^2\right\}}, \quad (12)$$

although these wave numbers differ because of the centrifugal term we note that a change ΔR in R can be made so as to result in $k_0(R+\Delta R) = k_L(R)$, that is,

$$\frac{1}{2}\mu\omega^2(R+\Delta R)^2 = \frac{1}{2}\mu\omega^2(R^2+2R\Delta R) = \frac{1}{2}\mu\omega^2 R^2 + \frac{\hbar^2 L(L+1)}{2\mu R^2},$$

$$\text{so that } \Delta R = \frac{\hbar^2 L(L+1)}{2\mu^2\omega^2 R^3}. \quad (13)$$

For the surface region of ^{222}Ra modeled as a ^{208}Pb core plus a ^{14}C cluster and with $L = 20$, $\mu \sim A_2 = 14$, $\hbar\omega \sim 41A_1^{-1/3} \sim 6.8$ MeV, and $R \sim 1.2A^{1/3}$ fm, we find $\Delta R \sim 0.10$ fm. Thus the classical turning points where the character of the wave functions changes from exponentially decreasing to oscillatory are grouped close together. Further into the internal region ΔR remains small and the wave functions remain approximately in phase. Of course, as R decreases further this ceases to be the case.

In summary, Eq. (13) tells us that ΔR decreases with decreasing L, with increasing R, and with increasing $\mu \sim A_2$, just as found in Fig. 1. We note that our chosen example of ^{222}Ra is something of a "worst case scenario," with a large difference in angular momenta and a small value of A_2. The radial wave functions will obviously be identical if the centrifugal potential can be ignored completely. The more closely this situation is approached, the greater their similarity.

III. GENERATING THE K BANDS

An eigenstate $\Psi^{JM}(\mathbf{R}, \boldsymbol{\xi})$ of the cluster-core system is a solution of the Schrödinger equation

$$H\Psi^{JM}(\mathbf{R}, \boldsymbol{\xi}) = E\Psi^{JM}(\mathbf{R}, \boldsymbol{\xi}), \quad (14)$$

TABLE I. Comparison of radial overlap integrals for ^{222}Ra, taking $2n + L = 70$, for wave functions generated numerically by solving the Schrödinger equation with the potential of Eqs. (2) and (3) (upper row of each pair) and for harmonic oscillator wave functions (lower row of each pair).

L	$L' = 0$	$L' = 2$	$L' = 4$	$L' = 6$	$L' = 8$	$L' = 10$	$L' = 12$	$L' = 14$	$L' = 16$	$L' = 18$	$L' = 20$
0	1	0.9849	0.9510	0.9009	0.8373	0.7632	0.6816	0.5957	0.5085	0.4230	0.3419
	1	0.9792	0.9324	0.8633	0.7770	0.6798	0.5780	0.4774	0.3830	0.2984	0.2255
2		1	0.9650	0.9134	0.8484	0.7728	0.6898	0.6026	0.5142	0.4276	0.3455
		1	0.9522	0.8816	0.7935	0.6942	0.5902	0.4876	0.3912	0.3047	0.2303
4			1	0.9452	0.8767	0.7976	0.7113	0.6209	0.5295	0.4402	0.3557
			1	0.9258	0.8333	0.7290	0.6199	0.5120	0.4108	0.3200	0.2419
6				1	0.9254	0.8405	0.7485	0.6526	0.5562	0.4622	0.3735
				1	0.9001	0.7875	0.6695	0.5531	0.4437	0.3456	0.2613
8					1	0.9057	0.8048	0.7008	0.5967	0.4957	0.4006
					1	0.8749	0.7439	0.6145	0.4930	0.3840	0.2903
10						1	0.8858	0.7696	0.6544	0.5434	0.4394
						1	0.8502	0.7023	0.5635	0.4389	0.3318
12							1	0.8658	0.7347	0.6095	0.4928
							1	0.8260	0.6627	0.5162	0.3902
14								1	0.8455	0.7002	0.5659
								1	0.8023	0.6239	0.4724
16									1	0.8251	0.6660
									1	0.7789	0.5888
18										1	0.8044
										1	0.7559
20											1
											1

TABLE II. Comparison of radial overlap integrals for ^{236}Pu, taking $2n + L = 140$, for wave functions generated numerically by solving the Schrödinger equation with the potential of Eqs. (2) and (3) (upper row of each pair) and for harmonic oscillator wave functions (lower row of each pair).

L	$L' = 0$	$L' = 2$	$L' = 4$	$L' = 6$	$L' = 8$	$L' = 10$	$L' = 12$	$L' = 14$	$L' = 16$	$L' = 18$	$L' = 20$
0	1	0.9927	0.9760	0.9510	0.9183	0.8791	0.8343	0.7849	0.7317	0.6758	0.6180
	1	0.9895	0.9653	0.9285	0.8805	0.8232	0.7588	0.6896	0.6178	0.5455	0.4749
2		1	0.9830	0.9574	0.9243	0.8846	0.8392	0.7893	0.7356	0.6792	0.6210
		1	0.9756	0.9384	0.8899	0.8320	0.7669	0.6969	0.6243	0.5514	0.4800
4			1	0.9734	0.9391	0.8982	0.8517	0.8006	0.7459	0.6884	0.6292
			1	0.9619	0.9122	0.8528	0.7861	0.7144	0.6400	0.5652	0.4920
6				1	0.9638	0.9210	0.8726	0.8196	0.7631	0.7039	0.6431
				1	0.9483	0.8867	0.8173	0.7427	0.6654	0.5876	0.5115
8					1	0.9543	0.9030	0.8474	0.7883	0.7267	0.6635
					1	0.9350	0.8618	0.7832	0.7016	0.6196	0.5394
10						1	0.9447	0.8852	0.8225	0.7576	0.6912
						1	0.9218	0.8377	0.7504	0.6627	0.5769
12							1	0.9351	0.8675	0.7980	0.7275
							1	0.9087	0.8141	0.7189	0.6258
14								1	0.9256	0.8499	0.7738
								1	0.8959	0.7913	0.6887
16									1	0.9159	0.8324
									1	0.8831	0.7687
18										1	0.9063
										1	0.8705
20											1
											1

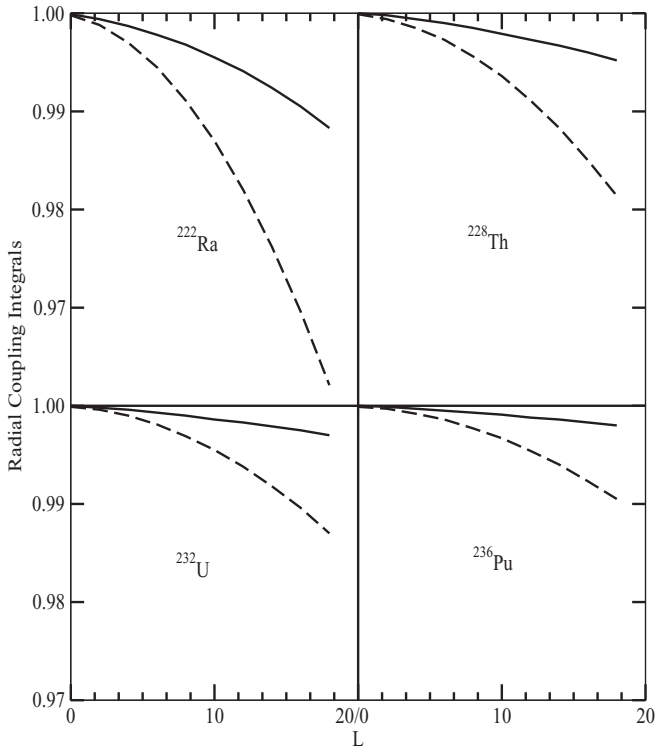

FIG. 2. Radial coupling integrals for radial wave functions whose L values differ by 2, (i.e., $\langle n, L|R \times \frac{dV}{dR}|n-1, L+2\rangle$) for the actinide nuclei ^{222}Ra, ^{228}Th, ^{232}U, and ^{236}Pu modeled as ^{208}Pb + ^{14}C, ^{20}O, ^{24}Ne, and ^{28}Mg, respectively. The solid lines represent results using wave functions obtained from a numerical solution of the Schrödinger equation with the potential of Eqs. (2) and (3) and the broken lines are equivalent harmonic oscillator results using Eq. (9). For ease of comparison, the values are given as ratios to the value obtained for $L = 0,\ L' = 0$.

where the Hamiltonian H is given by

$$H(\mathbf{R}, \boldsymbol{\xi}) = H_0(\mathbf{R}) + H_1(\boldsymbol{\xi}) + V(|\mathbf{R} - \boldsymbol{\xi}|). \tag{15}$$

Here $\mathbf{R}$ represents the cluster-core separation vector, and $\boldsymbol{\xi}$ represents the core's internal coordinates, which in the simplest cases might be no more than a linear superposition of the position vectors of its constituent nucleons. In Eq. (15) $H_0(\mathbf{R})$ is the Hamiltonian of the relative motion of A_1 and A_2 and $H_1(\boldsymbol{\xi})$ is the Hamiltonian of the core. The Schrödinger equation for $H_0(\mathbf{R})$ is given by Eq. (4) and that for $H_1(\boldsymbol{\xi})$ by Eq. (5), while a standard multipole expansion yields

$$V(|\mathbf{R} - \boldsymbol{\xi}|) = \sum_Q V_Q(R, \xi) C_Q(\hat{\mathbf{R}}) \cdot C_Q(\hat{\boldsymbol{\xi}}), \tag{16}$$

where $C_{Qq} \equiv \sqrt{4\pi/(2Q+1)}Y_{Qq}$. We first consider a single multipole Q in the expansion of Eq. (16), and a single core state χ_I in Eq. (5), and discuss later how these conditions may be relaxed.

Expanding $\Psi^{JM}(\mathbf{R}, \boldsymbol{\xi})$ in the coupled basis states in which the orbital angular momentum L combines with a core excitation of spin I to yield a total angular momentum J, we have

$$\Psi^{JM}(\mathbf{R}, \boldsymbol{\xi}) = \sum_{L'} a^J_{L'} [\Phi_{L'}(\mathbf{R}) \otimes \chi_I(\boldsymbol{\xi})]^{JM}. \tag{17}$$

Substituting from Eq. (17) for $\Psi^{JM}(\mathbf{R}, \boldsymbol{\xi})$ into Eq. (14), premultiplying by $[\Phi_L(\mathbf{R}) \otimes \chi_I(\boldsymbol{\xi})]^{JM}$, and integrating over $\mathbf{R}$ and $\boldsymbol{\xi}$ yields the eigenvalue equation

$$[E_L + \epsilon_I] a^J_L + \sum_{L'} V^J_{L,L'} a^J_{L'} = E a^J_L, \tag{18}$$

where we write

$$V^J_{L,L'} = \langle [\Phi_L(\mathbf{R}) \otimes \chi_I(\boldsymbol{\xi})]^{JM} | V_Q(R, \xi) C_Q(\hat{\mathbf{R}}) \cdot C_Q(\hat{\boldsymbol{\xi}}) | \times [\Phi_{L'}(\mathbf{R}) \otimes \chi_I(\boldsymbol{\xi})]^{JM} \rangle. \tag{19}$$

The integration over R yields explicitly

$$V^J_{L,L'} = \left\langle [Y_L(\theta, \phi) \otimes \chi_I(\boldsymbol{\xi})]^{JM} \left| W_Q^{L,L'}(\xi) C_Q(\hat{\mathbf{R}}) \cdot C_Q(\hat{\boldsymbol{\xi}}) \right| \times [Y_{L'}(\theta, \phi) \otimes \chi_I(\boldsymbol{\xi})]^{JM} \right\rangle, \tag{20}$$

and on introducing the reduced matrix elements [30]

$$V^J_{L,L'} = \langle [Y_L(\theta, \phi) \otimes \chi_I(\boldsymbol{\xi})]^{J} || W_Q^{L,L'}(\xi) C_Q(\hat{\mathbf{R}}) \cdot C_Q(\hat{\boldsymbol{\xi}}) || \times [Y_{L'}(\theta, \phi) \otimes \chi_I(\boldsymbol{\xi})]^{J} \rangle, \tag{21}$$

where we use Eq. (4) and define

$$W_Q^{L,L'}(\xi) = \int u_L(R) V_Q(R, \xi) u_{L'}(R) dR. \tag{22}$$

The crucial point here is that for similar radial wave functions $u_L(R)$ the radial integrals are almost independent of L so that

$$\int u_L(R) V_Q(R, \xi) u_{L'}(R) dR = W_Q^{L,L'}(\xi) = W_Q(\xi). \tag{23}$$

The reduced matrix element in Eq. (21) may therefore be replaced [30] via Eqs. (22) and (23) so that

$$\begin{aligned} V^J_{L,L'} &= (-1)^{J-L-I} \hat{L} \hat{I} W(LL'II; QJ) \langle Y_L || C_Q(\hat{\mathbf{R}}) || Y_{L'} \rangle \\ &\quad \times \langle \chi_I(\boldsymbol{\xi}) || W_Q(\xi) C_Q(\hat{\boldsymbol{\xi}}) || \chi_I(\boldsymbol{\xi}) \rangle \\ &= (-1)^{J-L-I} \hat{L}' \hat{I} W(LL'II; QJ) \langle L'0Q0|L0) \rangle \\ &\quad \times \langle \chi_I(\boldsymbol{\xi}) || W_Q(\xi) C_Q(\hat{\boldsymbol{\xi}}) || \chi_I(\boldsymbol{\xi}) \rangle, \end{aligned} \tag{24}$$

where we put $\hat{k} = \sqrt{(2k+1)}$ and so on.

We first consider the degenerate case where the energies E_L of the relative motion of the cluster and core are all equal. Choosing the zero of energy such that $E_L + \epsilon_I = 0$ we diagonalize $V^J_{L,L'}$ of Eq. (24) to obtain the coefficients a^J_L and eigenenergies E of Eq. (18). This can be done analytically [6] to yield

$$a^J_L \equiv a^J_{LK} = \frac{\hat{L}}{\hat{J}} \langle L0IK|JK \rangle, \tag{25}$$

and

$$E \equiv E_K = \langle IKQ0|IK \rangle \langle \chi_I(\boldsymbol{\xi}) || W_Q(\xi) C_Q(\hat{\boldsymbol{\xi}}) || \chi_I(\boldsymbol{\xi}) \rangle. \tag{26}$$

We note that in Eq. (17) we have summed over all L'. The restriction to the physical states $L^\pi = 0^+, 2^+, 4^+, \ldots,$

of the ground-state band requires the insertion of the factor $\frac{1}{2}[1+(-1)^{L'}]$ in Eq. (17) with the result that

$$\Psi^{JM}_{|K|}(\mathbf{R},\boldsymbol{\xi}) = \sum_L \frac{[1+(-1)^L]}{2}\frac{\hat{L}}{\hat{J}}\langle L0IK|JK\rangle \times [\Phi_L(\mathbf{R})\otimes\chi_I(\boldsymbol{\xi})]^{JM} = \frac{1}{2}\sum_L \frac{\hat{L}}{\hat{J}}[\langle L0IK|JK\rangle + (-1)^{J-K}\langle L0I-K|J-K\rangle] \times [\Phi_L(\mathbf{R})\otimes\chi_I(\boldsymbol{\xi})]^{JM}. \quad (27)$$

For given $|K|$, Eqs. (24), (25), and (26) tell us that all states with $J \geqslant |K|$ have the same energy E_K. The different $|K| \leqslant I$ thus each correspond to a K band generated by coupling the excitation I of the even-even core to the cluster-core relative rotational motion.

A. Several multipoles Q

The a^J_L of Eq. (25) are independent of Q. Thus the same transformation that diagonalizes a particular multipole Q of the interaction diagonalizes all Q [6] and Eq. (26) can be replaced by

$$E \equiv E_K = \sum_Q \langle IKQ0|IK\rangle\langle\chi_I(\boldsymbol{\xi})||W_Q(\xi)C_Q(\hat{\boldsymbol{\xi}})||\chi_I(\boldsymbol{\xi})\rangle. \quad (28)$$

B. Several core states I

Here we are particularly interested in the case of a core that has a 0^+ ground state and an $I^\pi = 2^+$ excited state. Equations (17), (18), and (19) then generalize to

$$\Psi^{JM}(\mathbf{R},\boldsymbol{\xi}) = \sum_{L',I'} a^J_{L'I'}[\Phi_{L'}(\mathbf{R})\otimes\chi_{I'}(\boldsymbol{\xi})]^{JM}, \quad (29)$$

$$[E_L+\epsilon_I]a^J_{LI} + \sum_{L',I'} V^J_{LI,L'I'}a^J_{L'I'} = Ea^J_{LI}, \quad (30)$$

$$V^J_{LI,L'I'} = \langle[\Phi_L(\mathbf{R})\otimes\chi_I(\boldsymbol{\xi})]^{JM}|V_Q(R,\xi)C_Q(\hat{\mathbf{R}})\cdot C_Q(\hat{\boldsymbol{\xi}})| \times [\Phi_{L'}(\mathbf{R})\otimes\chi_{I'}(\boldsymbol{\xi})]^{JM}\rangle, \quad (31)$$

where [27]

$$V^J_{LL'II'} = i^{L'-L+I'-I}(-1)^{L+L'+J}\beta\hat{L}\hat{L}'\hat{I}\hat{I}' \times \langle L0L'0|20\rangle\langle I0I'0|20\rangle W(L'I'LI;J2), \quad (32)$$

and $\hat{L} = \sqrt{(2L+1)}$ and so on. [We note that in Eq. (32) we followed the phase convention of earlier works [27–32] with Y_L replaced by $i^L Y_L$]. The inclusion of more than one core state thus necessitates the diagonalization of a larger Hamiltonian matrix than was the case for a single core state I discussed in Sec. III.

IV. LIFTING THE DEGENERACY: STRONG AND WEAK COUPLING

In applications to real nuclei both the core excitations, with their different values of I, and the cluster-core rotational states, with their different values of L, will have unequal energies associated with them. In the limit of weak coupling, the wave functions of the resulting J states are obtained by coupling a single value of I with a single value of L. Then the resulting spectrum contains one set of states formed from $I = 0 \otimes L = 0, 2, 4, \ldots$, (so that $J = L$ and the associated excitation energies are very close to the values of E_L) and another set of states formed from $I = 2 \otimes L = 0, 2, 4, \ldots$, (so that $J = L \pm 2$, $L \pm 1$, and L which are nearly degenerate with each other and displaced from the first set of states by roughly ϵ_I). That is to say, the weak coupling potential(s) V_Q have minimal effect on the states and their excitation energies. The situation is just like LS coupling in atomic physics.

At the other extreme, where the coupling potential matrix elements are very large compared to the excitation energies E_L and ϵ_I, we obtain the wave functions of the previous section consisting of combinations of I with several values of L and coefficients a^J_{LIK}. With unequal values of E_L and ϵ_I, the states are no longer degenerate, but rather spread out into distinctly recognizable bands, labeled by K. So there is a $K^\pi = 0^+$ band associated with the coupling of the $I^\pi = 0^+$ excitation to all the different L values and a further three bands labeled by $K^\pi = 0^+$, 1^+, and 2^+ associated with the coupling of the $I^\pi = 2^+$ excitation to the L values. For an attractive quadrupole-quadrupole coupling potential the ordering by excitation energy of the K bands in the strong coupling limit is $K^\pi = 0^+$, 0^+, 1^+, and 2^+, and for a repulsive potential it is $K^\pi = 0^+$, 2^+, 1^+, and 0^+. Of course, this may be modified by higher-order multipole interactions.

In real nuclei the situation is likely to lie between these two extremes and involve some kind of intermediate strength coupling. A full diagonalization of the Hamiltonian matrix for each J value is necessary, with the final result hopefully coming out close enough to the strong coupling limit for the labeling in terms of K to still be useful. This is clearly seen in the cases of ^{16}O [27], ^{24}Mg [28], and ^{40}Ca [29] when coupled-channels calculations are carried out including 0^+ ground and 2^+ excited states of the core. It is interesting to note that in these cases the energies of the $K^\pi = 1^+$ band are staggered so that they fall on either side of the collective-rotational model dependence on $L(L+1) - K^2$, whereas the other K-band energies follow the rotational model values much more closely.

We expect a similar situation to hold in heavier even-even nuclei as well. Although many $K^\pi = 0^+$ and $K^\pi = 2^+$ excited beta and gamma bands are seen in actinide nuclei there are no convincing identifications of any low-lying $K^\pi = 1^+$ bands. We predict that if the mechanism for band production is the coupling of a 2^+ state to a rotor with dominant quadrupole-quadrupole coupling then a $K^\pi = 1^+$ band ought to lie very close to the beta and gamma bands (whatever the sign of the coupling potential). Possible reasons for missing them so far include the following.

(i) It is intrinsically difficult to see nonnatural parity states in experiments, so the 1^+ bandhead is easily missed, leading to a $K^\pi = 1^+$ band being mistaken for a $K^\pi = 2^+$ band.

(ii) Coulomb excitation from the predominantly $|[I^\pi = 0^+ \otimes L = 0]\ 0^+\rangle$ ground state can take place in a

single step to the excited 2^+ bandhead through Y_2 operators acting on either the core or relative motion coordinates. This is mainly because of admixtures of $|[I^\pi = 2^+ \otimes L = 0]\ 2^+\rangle$ (the principal component of the 2^+ bandhead) and $|[I^\pi = 0^+ \otimes L = 2]\ 2^+\rangle$ in the excited 2^+ state. However, Coulomb excitation of the excited 0^+ and 1^+ bandheads cannot proceed so readily. The 0^+ ground state

$$|J^\pi = 0^+\rangle_{\text{g.s.}} = \alpha|[I^\pi = 0^+ \otimes L = 0]\ 0^+\rangle + \sqrt{1-\alpha^2}|[I^\pi = 2^+ \otimes L = 2]\ 0^+\rangle, \quad (33)$$

where the amplitude $\alpha \sim 1$, is orthogonal to the excited 0^+ bandhead wave function

$$|J^\pi = 0^+\rangle_{\text{ex.}} = \sqrt{1-\alpha^2}|[I^\pi = 0^+ \otimes L = 0]\ 0^+\rangle - \alpha|[I^\pi = 2^+ \otimes L = 2]\ 0^+\rangle, \quad (34)$$

and so cannot connect to it via a monopole interaction. This means that the transition can only proceed from the minority component of the ground state, or via a two-step process, involving Y_2 operators. Similarly, the 1^+ bandhead consists of a single component

$$|J^\pi = 1^+\rangle_{\text{ex.}} = |[I^\pi = 2^+ \otimes L = 2]\ 1^+\rangle, \quad (35)$$

and so here again excitation from the minority component of the ground state or two-step processes involving Y_2 operators are needed to excite this bandhead from the ground state. Therefore, in both cases, we expect small Coulomb excitation transition probabilities.

(iii) An alternative method of examining spectra in heavy nuclei is through populating the nucleus at high angular momentum in a heavy-ion collision. Electromagnetic decays (stretched $E2$ transitions) down bands are readily seen in this way, but there is a tendency for the cascade of gamma rays to jump across to a different band before the bandhead of the initially populated sequence is reached. This counts against "easy" population of any $K^\pi = 1^+$ bandhead in heavy-ion reactions.

(iv) The staggering of the energies in the 1^+ band (as seen in ^{16}O [27], ^{24}Mg [28], ^{40}Ca [29], and similarly in the 1^- band in ^{238}U [31,32]) makes it difficult to identify the band when its behavior is unanticipated, in contrast to the 0^+ and 2^+ band energies, which follow the expectations of the collective-rotational model much more closely.

To illustrate better the staggering of the energies in the 1^+ band Fig. 3 shows a generic spectrum calculated with parameter values compatible with the actinide region. These values are chosen to place excited 0^+ and 2^+ states in the region of the systematically observed beta and gamma bandhead energies. The cluster-core rotational motion is described by $\alpha L(L+1)$ with $\alpha = 0.01$ MeV, the core 0^+ and 2^+ states are taken to be separated by $\epsilon = 0.8$ MeV, and an intermediate strength quadrupole-quadrupole interaction [27] specified by Eq. (32) with $\beta = -0.178$ MeV acts between cluster and core.

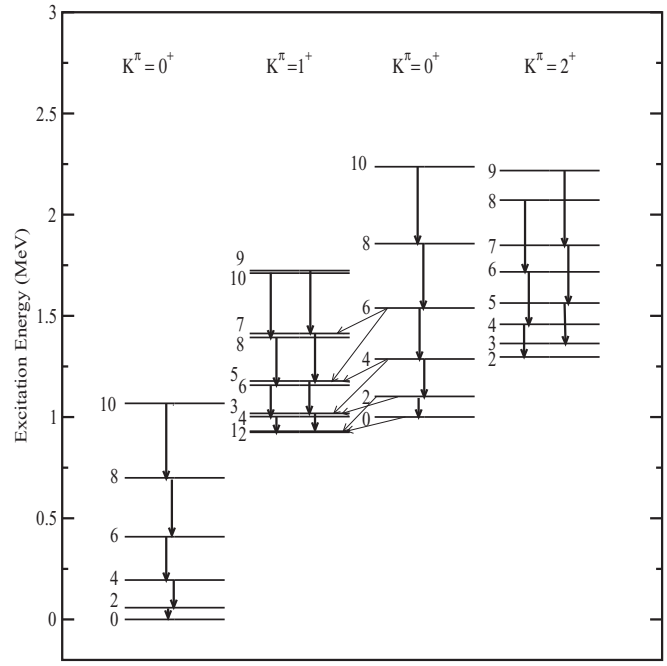

FIG. 3. Generic positive parity spectrum obtained by coupling a 0^+ ground state and an excited 2^+ state to a rotor. There are strong stretched $E2$ transitions within bands, weaker (typically by a factor of $\sim$10) unstretched $E2$ transitions between the excited $K^\pi = 0^+$ and the $K^\pi = 1^+$ bands, and weak but nonzero $M1$ transitions within the $K^\pi = 1^+$ and $K^\pi = 2^+$ bands, and between the $K^\pi = 0^+$ and the $K^\pi = 1^+$ bandheads (see text for details).

The resulting $K^\pi = 0^+, 2^+$, and 0^+ bands show excitation energies increasing with J albeit a little irregularly spaced. However, the $K^\pi = 1^+$ bands shows a sequence of inverted, nearly degenerate, doublets with 2^+ below 1^+, with 4^+ below 3^+, with 6^+ below 5^+, and so on. This model spectrum illustrates the potential difficulties that may arise in trying to identify from excitation energies alone a $K^\pi = 1^+$ band arising in the vicinity of $K^\pi = 0^+$ and 2^+ bands when the coupling strength is intermediate between the weak and strong limits. The precise details of the spectrum depend delicately on the strength of the noncentral interaction(s). The production of three excited K bands should be manifested by any model involving the coupling of a 2^+ excitation to a rotor, and is not dependent on an underlying cluster-core structure. Thus, if there are no symmetry considerations to be taken into account (such as identical boson restrictions, for example) a 1^+ state is a necessary consequence of coupling two 2^+ states together.

To summarize, the lack of observed $K^\pi = 1^+$ in heavy nuclei therefore presents a difficulty for our model, which needs to be addressed if the model is to provide a viable alternative to the Bohr-Mottelson picture of K bands. We note, however, that the model successfully describes the $K^\pi = 0^-, 1^-, 2^-$, and 3^- bands generated by an $I^\pi = 3^-$ excitation of the core [31,32] and we strongly urge our experimental colleagues to reexamine their data in heavier nuclei to see whether low-lying 1^+ bands in the vicinity of the 0^+ and 2^+ bands may have been missed. We note that in addition to direct observation of a 1^+ state, the finding of pairs of odd J^+ states

(i.e., 3^+, 5^+, 7^+, etc.) close together in the spectrum will also be supportive of our model. For example, ^{238}U has a (3^+) state at 1059.6617 keV and a 3^+ at 1105.71 keV.

V. ELECTROMAGNETIC TRANSITIONS

As a guide to reexamination of the spectra of heavy nuclei and an aid to experimentalists in this quest we discuss briefly the electromagnetic transitions expected from our model, indicated by the heavy and light arrows in Fig. 3. The differences from the collective-rotational model are not very great, but nevertheless significant.

Within each K band we predict stretched $E2$ transition strengths that are nearly related to that for the $2^+ \rightarrow 0^+$ transition in the ground-state band by Clebsch-Gordan coefficients. The in-band transitions between J and $J \pm 1$ are weaker than these by a factor typically between 5 and 10 (again, mainly because of angular momentum coupling coefficients). Most of the cross-band transitions are negligibly small. The exception to this statement is for the $E2$ transitions between the excited $K^\pi = 0^+$ band the the $K^\pi = 1^+$ band. The lower J members of these two bands are sufficiently mixed that the transitions between states with J and $J \pm 1$ are comparable to the unstretched in-band $E2$ transitions. These fairly strong $E2$ transitions do not persist beyond $J > 6$ in the example presented in Fig. 3.

Perhaps surprisingly the corresponding stretched $E2$ cross-band transitions are rather weak, typically a factor of 100 or more less than the in-band equivalents. The precise values, of course, depend on the exact parameter values used and the energetic proximity of the states to one another.

We also predict weak $M1$ transitions within the $K^\pi = 1^+$ and 2^+ bands. These will generally be swamped by the competing $E2$ transitions. They exist at all because the quadrupole-quadrupole interaction mixes components having the same I and the same L into states with J and $J \pm 1$ within a given band. One example, of potentially greater interest, is that we predict a weak $M1$ transition between the heads of the excited $K^\pi = 0^+$ and 1^+ bands. Although weak, this is not in competition with any other electromagnetic transition, so might be experimentally visible.

VI. CONCLUSION

We demonstrate, both numerically and analytically with reference to a three-dimensional simple harmonic oscillator potential, that the radial wave functions corresponding to states with a large, fixed value of $G = 2n + L$ are very closely similar, except in the vicinity of the origin. For the nuclei investigated, simple considerations taking into account the smallness of the centrifugal potential suggest that this near-identity is expected in the surface region. We show further that the integrals of these wave functions with a standard derivative form of the radial coupling potential are even more nearly equal to one another. This latter observation is particularly important for the cases of cluster-core states interacting through a low multipole (e.g., quadrupole-quadrupole) coupling potential. It provides a bridge between the geometric interpretation of K bands in terms of a fixed intrinsic state and the algebraic approach where these near-identical radial functions can play the same role.

The common situation where a core has both a 0^+ ground state and a low-lying 2^+ excited state leads to the generation of two $K^\pi = 0^+$ bands with additional $K^\pi = 1^+$ and $K^\pi = 2^+$ bands. If the dominant interaction between cluster and core is of quadrupole-quadrupole type, then the $K^\pi = 1^+$ band is expected to lie very close to the excited $K^\pi = 0^+$ and $K^\pi = 2^+$ bands. Although this behavior is observed in light nuclei, a number of reasons are suggested for it being generally difficult to see, so that it may have been missed altogether in heavier nuclei. The reexamination of existing data and, ideally, new purpose-driven experimental searches for low-lying $K^\pi = 1^+$ bands may prove profitable.

ACKNOWLEDGMENTS

S.M.P. would like to thank the S.A. Foundation for Research, and the University of Cape Town for financial support.

APPENDIX

The radial part of the three-dimensional harmonic oscillator wave function is given by

$$\phi_{nlm}(r/b) = \sqrt{\frac{2 \times (n)!}{\Gamma(n + l + 3/2) b^3}} \left(\frac{r}{b}\right)^l \times L_n^{l+3/2}(r^2/b^2) e^{-r^2/2b^2}, \tag{A1}$$

where b is the oscillator length parameter given by $b^2 = \hbar/\mu\omega$ and $L_n^{l+3/2}(r^2/b^2)$ is an associated Laguerre polynomial. Radial overlap integrals between states in the same band (i.e., having the same value of $2n + l + 3/2$) are thus given by

$$\begin{aligned} &\langle n, l | n - m, l + 2m \rangle \\ &\quad = I_{nl}^{(m)} = \sqrt{\frac{2 \times (n)!}{\Gamma(n + l + 3/2)} \frac{2 \times (n - m)!}{\Gamma(n + l + m + 3/2)}} \times \frac{1}{b^3} \\ &\quad \times \int_0^\infty \left(\frac{r}{b}\right)^l \left(\frac{r}{b}\right)^{l+2m} L_n^{l+1/2}\left(\frac{r^2}{b^2}\right) L_{n-m}^{l+2m+1/2}\left(\frac{r^2}{b^2}\right) \\ &\quad \times e^{-r^2/b^2} r^2 \, dr, \end{aligned} \tag{A2}$$

which may be evaluated with the help of the relation [33]

$$\begin{aligned} &\int_0^\infty e^{-x} x^s L_n^k(x) L_{n'}^{k'}(x) \, dx \\ &\quad = (s)! \sum_{r=0}^{\min(n,n')} (-1)^{n+n'+r} \binom{s-k}{n-r} \binom{s-k'}{n'-r} \binom{-s-1}{r}, \end{aligned} \tag{A3}$$

where

$$\begin{aligned} &\binom{n}{k} = \frac{(n)!}{(k)!(n-k)!} \text{ for } n \geqslant k \geqslant 0, \quad \text{but} \\ &\binom{n}{k} = 0 \text{ for } k > n > 0, \end{aligned} \tag{A4}$$

and

$$\binom{-n}{k} = (-1)^k \binom{(n+k-1)!}{(k)!} \text{ for } k > n > 0. \quad \text{(A5)}$$

There is only one nonzero contribution to the summation for the overlap integrals in Eq. (A2), coming from $r = n - 1$, and the integral simplifies to

$$I_{nl}^{(m)} = (-1)^m \sqrt{\frac{(n)!}{(n-m)!} \times \frac{\Gamma(n+l+3/2)}{\Gamma(n+l+m+3/2)}}. \quad \text{(A6)}$$

In a similar fashion, radial integrals for a coupling potential rdV/dr, where V is proportional to r^2, between harmonic oscillator wave functions for states in the same band may be evaluated analytically as

$$\langle n, l | r \frac{dV}{dr} | n-m, l+2m \rangle = \mu\omega^2 b^2 I_{nl}^{(m)} [(m+1)(n+l+3/2) - (m-1)(n-m)]. \quad \text{(A7)}$$

In this case the two terms having $r = n - m - 1$ and $r = n - m$ give (generally) nonzero contributions to the sum in Eq. (A3).

[1] Brookhaven National Nuclear Data Center at [http://www.nndc.bnl.gov/ensdf].
[2] D. R. Tilley, J. H. Kelley, J. L. Godwin, D. J. Millener, J. E. Purcell, C. G. Sheu, and H. R. Weller, Nucl. Phys. A **745**, 155 (2004).
[3] D. R. Tilley, H. R. Weller, and C. M. Cheves, Nucl. Phys. A **564**, 1 (1993).
[4] P. M. Endt, Nucl. Phys. A **521**, 1 (1990).
[5] A. Bohr and B. R. Mottelson, *Nuclear Structure* (Benjamin, New York, 1969), Vol. 2, p. 10.
[6] D. M. Brink, B. Buck, R. Huby, M. A. Nagarajan, and N. Rowley, J. Phys. G **13**, 629 (1987).
[7] A. Bohr and B. R. Mottelson, *Nuclear Structure* (Benjamin, New York, 1969), Vol. 2, p. 347
[8] K. Neergård and P. Vogel, Nucl. Phys. A **149**, 217 (1971).
[9] P. Vogel, Phys. Lett. B **60**, 431 (1976).
[10] D. Ward *et al.*, Nucl. Phys. A **600**, 88 (1996).
[11] A. A. Kuliev, E. Gugliev, F. Ertugral, and S. Ozkan, Eur. Phys. Jour. A **43**, 313 (2010).
[12] N. Minkov, S. Drenska, P. Yotov, and W. Scheid, Phys. At. Nucl. **67**, 1760 (2004).
[13] N. Minkov, P. Yotov, S. Drenska, and W. Scheid, J. Phys. G: Nucl. Part. Phys. **32**, 497 (2006).
[14] A. A. Raduta and C. M. Raduta, Nucl. Phys. A **768**, 170 (2006).
[15] N. V. Zamfir and D. Kusnezov, Phys. Rev. C **67**, 014305 (2003).
[16] P. D. Cottle and N. V. Zamfir, Phys. Rev. C **58**, 1500 (1998).
[17] D. Lenis and D. Bonatsos, Phys. Lett. B **633**, 474 (2006).
[18] T. Schneidman, G. G. Adamian, N. V. Antonenko, R. V. Jolos, and W. Scheid, Phys. Lett. B **526**, 322 (2002).
[19] B. Buck, A. C. Merchant, and S. M. Perez, Nucl. Phys. A **614**, 129 (1997).
[20] B. Buck, A. C. Merchant, and S. M. Perez, Phys. Rev. C **58**, 2049 (1998).
[21] B. Buck, A. C. Merchant, and S. M. Perez, Phys. Rev. Lett. **76**, 380 (1996).
[22] B. Buck, A. C. Merchant, and S. M. Perez, Phys. Rev. C **57**, R2095 (1998).
[23] Y. A. Akovali, Nucl. Data Sheets **77**, 271 (1996).
[24] A. Artna-Cohen, Nucl. Data Sheets **80**, 723 (1997).
[25] E. Browne, Nucl. Data Sheets **107**, 2579 (2006).
[26] E. Browne, Nucl. Data Sheets **107**, 2649 (2006).
[27] R. A. Baldock, B. Buck, and J. A. Rubio, Nucl. Phys. A **426**, 222 (1984).
[28] B. Buck, P. J. B. Hopkins, and A. C. Merchant, Nucl. Phys. A **513**, 75 (1990).
[29] A. C. Merchant, Phys. Rev. C **37**, 414 (1988).
[30] D. M. Brink and G. R. Satchler, *Angular Momentum*, 3rd ed. (Oxford University Press, Oxford, 1993), pp. 57, 78, and 151.
[31] B. Buck, A. C. Merchant, and S. M. Perez J. Phys. G: Nucl. Part. Phys. **35**, 085101 (2008).
[32] B. Buck, A. C. Merchant, S. M. Perez, T. T. Ibrahim, and S. M. Wyngaardt, J. Phys. G: Nucl. Part. Phys. **36**, 085101 (2009).
[33] A. Galindo and P. Pascual, *Quantum Mechanics* (Springer, Berlin, 1990), Vol. 1, p. 309